

Prescribed performance adaptive fault-tolerant trajectory tracking control for an ocean bottom flying node

International Journal of Advanced
Robotic Systems
May-June 2019: 1–13
© The Author(s) 2019
DOI: 10.1177/1729881419841943
journals.sagepub.com/home/arx



Hongde Qin , Zheyuan Wu, Yanchao Sun  and Yushan Sun

Abstract

The ocean bottom flying node is a novel autonomous underwater vehicle that explores the oil and gas resources in deep water. Thousands of the ocean bottom flying nodes track different predefined trajectories arriving at target points in a small ocean area, respectively. A class of prescribed performance adaptive trajectory tracking control method is investigated for the ocean bottom flying node trajectory tracking problem with ocean current disturbances, model uncertainties as well as thruster faults. Based on a predefined performance function and an error transformation, the ocean bottom flying node trajectory tracking error is restricted to prespecified bounds to ensure a desired transient and steady response. Radial basis function neural network is used to approximate the general uncertainty caused by ocean current disturbances, model uncertainties, and thruster faults. Further, the upper bound of approximation error is estimated by an adaptive law. Using the adaptive laws, we propose a prescribed performance adaptive trajectory tracking controller. The simulation examples on an ocean bottom flying node system show that the proposed control scheme can compensate for the effect of the general uncertainty while obtaining the fast transient process and expected trajectory tracking accuracy.

Keywords

Ocean bottom flying node, autonomous underwater vehicle, trajectory tracking control, prescribed performance, fault-tolerant control, neural network

Date received: 25 May 2018; accepted: 25 February 2019

Topic: Robot Manipulation and Control

Topic Editor: Yangquan Chen

Associate Editor: Shun-Feng Su

Introduction

In recent years, autonomous underwater vehicle (AUV) has been widely applied in the fields of marine environmental monitoring and military intelligence gathering.^{1–3} With the expansion of the ocean development scale, the applications of the AUVs gradually extend from observation to operation, such as underwater infrastructure inspection, deep-water oil, and gas exploration.^{4–7} The ocean bottom flying node (OBFN) is a kind of large-scale deployed AUV that equips the geophone and hydrophone to explore the oil and gas resources. Thousands of the OBFNs track different predefined trajectories arriving at target points in a small ocean area, respectively. Trajectory tracking is a fundamental element of the AUV control system.

However, highly nonlinear and cross-coupled characteristics of system dynamics, model uncertainties introduced by unpredictable underwater environment, and external disturbances bring challenges for the AUV control algorithms design.⁸ In addition, according to the complicated missions, the requirement for the control precision will be further

Science and Technology on Underwater Vehicle Laboratory, Harbin Engineering University, Harbin, China

Corresponding author:

Yanchao Sun, Science and Technology on Underwater Vehicle Laboratory, Harbin Engineering University, Harbin 15001, China.

Email: sunyanchao@hrbeu.edu.cn



increased. Ocean current which is a common disturbance in marine environment affects the control precision. Bi et al.⁹ proposed a trajectory tracking control strategy based on Lyapunov method and ocean current observer in the presence of unknown horizontal ocean current. This control algorithm was proven to be effective by means of cascaded system stability criterion. Kokegei et al.¹⁰ developed a fully coupled sliding mode control algorithm for AUV under the ocean current disturbance. This method was based on the maximum instantaneous cross-track error obtained during the trajectory tracking.

However, the above results are based on the condition that the AUV model parameters are known. In fact, the parameters which depend on the experimental data or the computational fluid dynamics (CFD) commercial software exist modeling errors. Therefore, it is more suitable to consider model uncertainties for the control laws design, which has actual engineering value. Previous studies^{11,12} used terminal sliding mode control schemes for the trajectory tracking of fully actuated AUVs in the presence of dynamic uncertainties and time-varying external disturbances. Londhe et al.¹³ proposed a trajectory tracking control method for a kind of AUV system with nonlinear and highly coupled dynamics based on the non-singular terminal sliding mode technique. The system states could converge to the origin in finite time when there existed model uncertainties. Wang et al.¹⁴ used universal fuzzy state observer and adaptive fuzzy approximators to observe unmeasured states and unknown dynamics, respectively. Rout and Subudhi¹⁵ investigated an adaptive proportional–integral–derivative (PID) controller using the derived parameters, which utilized the recursive extended least square algorithm to estimate model parameters online. Wang et al.¹⁶ developed an innovative retractable fuzzy approximator to estimate internal nonlinearities. Additionally, external unknowns are globally dominated by adaptive universal compensators. Karkoub et al.¹⁷ developed a robust nonlinear control strategy based on the backstepping and sliding mode control techniques to achieve the AUV trajectory tracking control and virtual velocity control when considering model uncertainties. Wang et al.¹⁸ constructed approximators based on the single-hidden-layer feedforward network to exactly dominate completely unknown dynamics. Lakhekar and Waghmare¹⁹ proposed an adaptive fuzzy PI sliding mode controller for the AUV in the complex oceanic environment and imprecise hydrodynamic coefficients. This control algorithm basically consisted of approximately known inverse dynamic model output and continuous adaptive PI term is developed to deal with chattering effect. Wang et al.²⁰ addressed a finite-time observer based accurate tracking control scheme for marine vehicle with complex unknowns including unmodeled dynamics and disturbances.

For the AUV model uncertainties, the above references developed many trajectory tracking control strategies which achieve satisfactory results. However, the above

research studies are all proposed without considering fault problems. Because of the complexity of the maritime environment, the AUV may break down in operation process, while the thruster fault is representative. Since this study investigates the trajectory tracking control for the OBFNs, which are applied for large-scale deployments, the thruster fault case is worth considering. Sun et al.²¹ proposed a tracking control method with thruster fault accommodation, which divided faults into part cases and complete cases and utilized a weighted pseudo-inverse operation to generate the new thrust allocation matrix. Ahmadzadeh et al.²² developed learning approaches for discovering fault-tolerant control method to deal with thruster fault. This method employed a multi-objective reinforcement learning approach to discover a set of optimal solutions and to handle multiple conflicting objectives. Davoodi et al.²³ proposed an H_∞/H_- formulation using a dynamic observer which achieved the simultaneous fault detection, isolation, and tracking problem for linear continuous-time systems.

It can be found that the research approaches of the above studies individually designed fault detection and diagnosis units for the AUVs. Wang et al.²⁴ considered the thruster fault as a part of the general uncertainty which also included the model uncertainty and external disturbance. In addition, radial basis function neural network (RBFNN) was adopted to approximate the general uncertainty. This way is more suitable to deal with thruster fault and appropriate for complex AUV models. Zhang et al.²⁵ investigated a fault-tolerant control method for AUVs with thruster fault based on adaptive terminal sliding mode technique. Moreover, the adaptive law was introduced to estimate the upper bounds of system uncertainty which included ocean current disturbances, model uncertainties, and thruster faults. Zhang et al.²⁶ developed a type of piecewise and differential Lyapunov function to achieve region tracking control based on the frame of backstepping technique. An adaptive technique is used to estimate the unknown coefficients of the lumped uncertainty.

For the specific task requirements of the OBFN, including large-scale deployments and high accuracy trajectory tracking as well as landing on the seabed, controller design of each AUV should not only consider ocean current disturbances, model uncertainties, and thruster faults but also suppress the overshoot to avoid collisions with each other in the deployment process. Although the above references realized trajectory tracking control in different disturbances, the final trajectory tracking precision depended on controller capabilities or selections of control gains. Bechlioulis and Rovithakis proposed a prescribed performance control theory in 2008.²⁷ The theory transforms the constrained system into an equivalent unconstrained system to obtain prescribed performance, including rate of convergence, tracking error, and overshoot, by means of an appropriately defined output error transformation. The prescribed performance control theory has been applied in some fields, such as servosystem,²⁸ flexible air-breathing

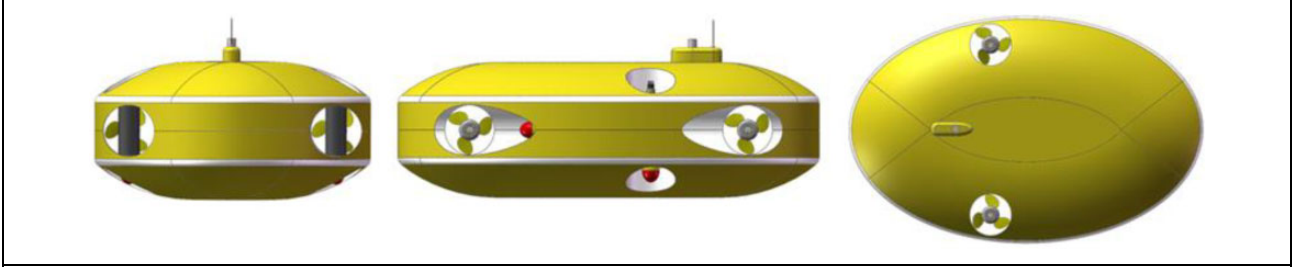


Figure 1. The OBFN system. OBFN: ocean bottom flying node.

hypersonic vehicle,²⁹ stochastic systems,³⁰ and underactuated underwater vehicles.³¹ This study proposes an adaptive neural network controller based on the prescribed performance control theory for trajectory tracking for a class of the OBFN AUVs. The RBFNN is adopted to approximate the general uncertainty including ocean current disturbances and model uncertainties as well as thruster faults. In addition, adaptive method is applied to estimate the upper bound of the approximate error. Based on performance function and an error transformation, the system trajectory tracking error is restricted to prescribed bounds to ensure a desired transient and steady response. The simulation results indicate that the proposed method can deal with the effect of model uncertainties, ocean current disturbances, and thruster faults while obtaining an expected trajectory tracking accuracy. In comparison to the existing works, the main contributions of this study are shown as follows:

- (1) To fulfill potency of prescribed performance method, we use it to deal with trajectory tracking control for the OBFN which has higher requirements for control precision and convergence process of tracking error.
- (2) The consideration for many influence factors including ocean current disturbances, modeling uncertainties, and thruster faults are not quite comprehensive in published works. In this study, we introduce the system general uncertainties to replace these factors. It is easier to be used in engineering practice.
- (3) This study introduces the RBFNN to approximate the general uncertainties. To overcome restrictive condition of unknown detailed parameters, adaptive method is applied to estimate the upper bound of the approximate error.

The subsequent contents in this article are as follows: second section presents modeling processes of the OBFN dynamic model including disturbances, uncertainties, and faults. “Prescribed performance control” section introduces prescribed performance method and error transformation. The design and proving processes of the prescribed performance adaptive trajectory tracking controller are given in “The design of adaptive trajectory tracking controller”

section. Fourth section shows the corresponding simulation results for two types of thruster fault.

Preliminaries

Concepts of the OBFN

To meet the needs of deep water seismic observation, the ocean bottom node (OBN) was developed which can provide excellent illumination with complete uniform azimuth distribution for complex imaging in deep water.^{32–34} However, seismic detection nodes in existing OBN systems were usually placed or recovered individually using a remotely operated vehicle (ROV). Thus, there was inefficiency as to the deployment and recovery of seismic survey.

To overcome the limitations of OBN, this article proposes an OBFN that combines the OBN and AUV techniques, as shown in Figure 1. It can cruise to the designated deep water location and remain static at the seafloor to acquire long-term seismic data. Without the requirement of ROVs during the deployment and recovery process, it would provide dramatic time and cost savings for ocean bottom seismic operations. Thus the OBFN retains all the advantages of OBN systems, while at the same time is much more flexible and maneuverable than traditional OBNs. Since the seismic experiment requires tens of thousands of OBFNs to be deployed within a short period of time, the trajectory tracking of OBFN networks is a challenging problem. Not only should we consider ocean current disturbances, model uncertainties, and thruster faults but also control overshoot to avoid bumping into each other in the deployment process. In this research, the trajectory tracking of OBFN swarms will be achieved by extension of an adaptive neural network controller based on the prescribed performance technique.

Dynamics model of the OBFN

The dynamic model for the OBFN system can be expressed as³⁵

$$M_\eta \ddot{\eta} + C_{RB\eta} \dot{\eta} + C_{A\eta} \dot{\eta}_r + D_\eta \dot{\eta}_r + g_\eta = \tau \quad (1)$$

where $M_\eta = MJ^{-1}$, $C_{RB\eta} = [C_{RB}(v) - MJ^{-1}\dot{J}]J^{-1}$, $C_{A\eta} = C_A(v_r)J^{-1}$, $D_\eta = D(v_r)J^{-1}$, $g_\eta = g(\eta)$, $\dot{\eta}_r = J(\eta)v_r$, and

$v_r = v - v_c$. M is the inertial matrix including the added mass, $\eta = [x, y, z, \phi, \theta, \psi]^T$ is the position and orientation vector in the earth-fixed frame, $v = [u, v, w, p, q, r]^T$ is the velocity vector in the body-fixed frame, J is the transformation matrix between the earth-fixed frame and the body-fixed frame, C_{RB} is the rigid-body Coriolis and Centripetal matrix, C_A is the added Coriolis and Centripetal matrix, D is the drag coefficient matrix, g_η is the vector of gravitational/buoyancy forces and moments, and τ is the control forces and moments acting on the OBFN. v_r is the vehicle velocity relative to ocean current, and v_c is the ocean current velocity in the body-fixed frame.

Thruster, an important part of the AUV, is the main resource of faults.³⁶ The variation of thrust allocation matrix is adopted to represent the effect of thruster fault, denoted as ΔB . Therefore, the real control force/moment is changed to $\tau + \Delta\tau$.²⁶

$$\tau + \Delta\tau = (B_0 - K_1 B)u = (B_0 + \Delta B)u \quad (2)$$

where B_0 is the nominal value of the thrust allocation matrix, u is the control input of thrusters, and K_1 is a diagonal matrix while the element $k_{ii} \in [0, 1]$, which represents the level of the corresponding thruster fault. Therefore, equation can be transformed as

$$\ddot{\eta} = M_{\eta 0}^{-1}(B_0 u - C_{RB\eta 0} \dot{\eta} - C_{A\eta 0} \dot{\eta} - D_{\eta 0} \dot{\eta} - g_{\eta 0}) - F \quad (3)$$

where subscript '0' denotes the nominal value. F is the system general uncertainty expressed as

$$F = M_{\eta 0}^{-1}(\Delta M_\eta \ddot{\eta} - \Delta B u + \Delta C_{RB\eta} \dot{\eta} + \Delta C_{A\eta} \dot{\eta} + \Delta D_\eta \dot{\eta} + \Delta g_\eta + \overline{C_{A\eta} \eta_r + D_\eta \eta_r}) \quad (4)$$

where $\overline{C_{A\eta} \eta_r + D_\eta \eta_r}$ denotes the effect of ocean current disturbance, and Δ denotes the uncertainty.

The objective of this study is to design a control strategy for the OBFN to track the desired trajectory and to ensure a desired transient and steady response of the tracking error when considering system uncertainty and thruster fault.

We make the following assumptions based on practical project background.

Assumption 1. The trajectory vector η and its first derivative are available for measurement.

Assumption 2. The desired trajectory η_d and its first and second derivatives are known bounded functions.

Remark 1. Owing to $\dot{\eta} = J(\eta)v$, the first derivative of trajectory vector η can be calculated by the velocity vector v in the body-fixed frame. Then the Assumption 1 is equivalent that η and v are available for measurement.

Remark 2. The OBFN need track predefined trajectory to arrive at target point. Therefore, the trajectory is known,

and then its first and second derivatives are known and bounded.

The OBFN trajectory tracking control law design

Prescribed performance control

The performance function can be defined as follows.

Definition 1. A smooth function $\rho(t): \mathbb{R}_+ \rightarrow \mathbb{R}$ will be called a performance function if²⁷.

1. $\rho(t)$ is decreasing and positive and
2. $\lim_{t \rightarrow \infty} \rho(t) = \rho_\infty > 0$

The performance function is usually designed as follows

$$\rho(t) = (\rho_0 - \rho_\infty)e^{-kt} + \rho_\infty \quad (5)$$

where ρ_0, ρ_∞ , and k are preset positive constants.

Based on performance function, the tracking error can be expressed as follows

$$\begin{aligned} -\delta_i \rho_i(t) < e_i(t) < \rho_i(t), e_i(0) \geq 0; \\ -\rho_i(t) < e_i(t) < \delta_i \rho_i(t), e_i(0) < 0 \end{aligned} \quad (6)$$

where $e_i(t)$, $i = 1 - 6$ denotes the i th trajectory tracking error of the OBFN in the earth-fixed frame, $0 \leq \delta_i \leq 1$. If the initial value of the tracking error $e_i(t)$ satisfies $0 \leq |e_i(0)| < \rho_i(0)$, the parameter k_i regulates the minimum convergence speed of tracking error $e_i(t)$ and the terminal value of the performance function ρ_∞ restrains the maximum bound of steady state tracking error. Therefore, the expected tracking error can be obtained by designing appropriate $\rho_i(t)$.

To solve prescribed performance control problem represented by equation (6), this research adopts an error transformation to transform the constrained trajectory tracking control problem into an equivalent unconstrained one. We define a function $S_i(\varepsilon_i)$:

- (1) $S_i(\varepsilon_i)$ is smooth and strictly increasing

- (2) $-\delta_i < S_i(\varepsilon_i) < 1, e_i(0) \geq 0$
 $-1 < S_i(\varepsilon_i) < \delta_i, e_i(0) < 0$

- (3) $\left. \begin{aligned} \lim_{\varepsilon_i \rightarrow -\infty} S_i(\varepsilon_i) &= -\delta_i \\ \lim_{\varepsilon_i \rightarrow +\infty} S_i(\varepsilon_i) &= 1 \end{aligned} \right\}, e_i(0) \geq 0,$
 $\left. \begin{aligned} \lim_{\varepsilon_i \rightarrow -\infty} S_i(\varepsilon_i) &= -1 \\ \lim_{\varepsilon_i \rightarrow +\infty} S_i(\varepsilon_i) &= \delta_i \end{aligned} \right\}, e_i(0) < 0$

where $\varepsilon_i \in (-\infty, +\infty)$ denotes the transformed error. A function $S_i(\varepsilon_i)$ which satisfies the above conditions can be expressed as

$$S_i(\varepsilon_i) = \begin{cases} \frac{e^{\varepsilon_i} - \delta_i e^{-\varepsilon_i}}{e^{\varepsilon_i} + e^{-\varepsilon_i}}, & e_i(0) \geq 0 \\ \frac{\delta_i e^{\varepsilon_i} - e^{-\varepsilon_i}}{e^{\varepsilon_i} + e^{-\varepsilon_i}}, & e_i(0) < 0 \end{cases} \quad (7)$$

From the characteristic of $S_i(\varepsilon_i)$, equation (6) can be equivalently expressed as

$$e_i(t) = \rho_i(t) S_i(\varepsilon_i) \quad (8)$$

Owing to the strictly increasing properties of $S_i(\varepsilon_i)$, there exists an inverse function expressed as follows

$$\varepsilon_i = S_i^{-1} \left(\frac{e_i(t)}{\rho_i(t)} \right) \quad (9)$$

If we are able to keep ε_i bounded, then we can guarantee that equation (6) is satisfied. Owing to the constraint of prescribed performance $\rho_i(t)$, the tracking error could obtain expectation objective. The trajectory tracking control problem of equation (3) can be transformed into the stabilization control problem of closed-loop system with respect to variable ε_i .

We define $S_i(\varepsilon_i)$ equivalently to the form of equation (7), then

$$\varepsilon_i = S_i^{-1} \left(\frac{e_i(t)}{\rho_i(t)} \right) = \begin{cases} \frac{1}{2} \ln \frac{z_i + \delta_i}{1 - z_i}, & e_i(0) \geq 0 \\ \frac{1}{2} \ln \frac{1 + z_i}{\delta_i - z_i}, & e_i(0) < 0 \end{cases} \quad (10)$$

where $z_i = e_i(t)/\rho_i(t)$.

Remark 3. From equation (10), δ_i cannot be chosen equal to zero with $e_i(0) = 0$, otherwise $\varepsilon_i(0)$ will tend to infinity.

Differentiating equation (10) with respect to time, we have

$$\dot{\varepsilon}_i = \frac{\partial S_i^{-1}}{\partial z_i} \cdot \dot{z}_i = \frac{\partial S_i^{-1}}{\partial z_i} \cdot \frac{\dot{e}_i \rho_i - e_i \dot{\rho}_i}{\rho_i \cdot \rho_i} = r_i \left(\dot{e}_i - \frac{e_i \dot{\rho}_i}{\rho_i} \right) \quad (11)$$

where $r_i = (\partial S_i^{-1} / \partial z_i) \cdot (1/\rho_i)$ by calculation of equation (10). r_i is positive because of $(\partial S_i^{-1} / \partial z_i) > 0$ and $\rho_i(t) > 0$. In addition, r_i is bounded, $\underline{r} < r_i < \bar{r}$, when trajectories of the error $e_i(t)$ be limited to the bounds of equation (6), where \underline{r} and \bar{r} are positive constants.

Differentiating equation (11) with respect to time, we have

$$\begin{aligned} \ddot{\varepsilon}_i &= \dot{r}_i \left(\dot{e}_i - \frac{e_i \dot{\rho}_i}{\rho_i} \right) + r_i \left(\ddot{e}_i - \frac{\dot{e}_i \dot{\rho}_i \rho_i + e_i \ddot{\rho}_i \rho_i + e_i \dot{\rho}_i^2}{\rho_i^2} \right) \\ &= \dot{r}_i \left(\dot{e}_i - \frac{e_i \dot{\rho}_i}{\rho_i} \right) - r_i \cdot \frac{\dot{e}_i \dot{\rho}_i \rho_i + e_i \ddot{\rho}_i \rho_i + e_i \dot{\rho}_i^2}{\rho_i^2} \\ &\quad + r_i (\ddot{\eta}_i - \ddot{\eta}_{di}) \end{aligned} \quad (12)$$

where $\ddot{\eta}_i, \ddot{\eta}_{di}$, $i = 1, 2, 3, 4, 5, 6$ denote actual and desired trajectories for the OBFN, respectively.

The error variance $s \in \mathbb{R}^6$ can be denoted as follows

$$s = \lambda \varepsilon + \dot{\varepsilon} \quad (13)$$

where $\varepsilon = [\varepsilon_1, \varepsilon_2, \varepsilon_3, \varepsilon_4, \varepsilon_5, \varepsilon_6]^T$ and $\lambda = \text{diag}[\lambda_1, \lambda_2, \lambda_3, \lambda_4, \lambda_5, \lambda_6] > 0$ are predefined design parameters. According to dynamic model (3) for the OBFN

$$\dot{\eta} = M_{\eta 0}^{-1} (B_0 u - C_{RB\eta 0} \dot{\eta} - C_{A\eta 0} \dot{\eta} - D_{\eta 0} \dot{\eta} - g_{\eta 0}) - F$$

where $A = -M_{\eta 0}^{-1} [(C_{RB\eta 0} \dot{\eta} + C_{A\eta 0} \dot{\eta} + D_{\eta 0} \dot{\eta}) \dot{\eta} + g_{\eta 0}]$, $H = M_{\eta 0}^{-1} B_0$, and $D = -F$. Equation (3) can be expressed as

$$\dot{\eta} = A + H u + D \quad (14)$$

In addition,

$$\dot{s} = \lambda \dot{\varepsilon} + \ddot{\varepsilon} = L + R(A + H u + D) \quad (15)$$

where $L = [l_1, l_2, l_3, l_4, l_5, l_6]^T$, $l_i = (\lambda_i r_i + \dot{r}_i) \left(\dot{e}_i - \frac{e_i \dot{\rho}_i}{\rho_i} \right) - r_i \cdot \frac{\dot{e}_i \dot{\rho}_i \rho_i + e_i \ddot{\rho}_i \rho_i + e_i \dot{\rho}_i^2}{\rho_i^2} - r_i \ddot{\eta}_{di}$, $i = 1 - 6$, and $R = \text{diag}[r_1, r_2, r_3, r_4, r_5, r_6]$. If we design a controller u to guarantee s to be bounded, then ε_i and $\dot{\varepsilon}$ are also bounded.

The design of adaptive trajectory tracking controller

We utilize the capabilities of the RBFNN to approximate uncertain nonlinearity D in the system (14)³⁷

$$D = W^* h(x) + \mu \quad (16)$$

where $x \in \mathcal{Q}_x \subset \mathbb{R}^q$ is RBFNN input vector, $h(x) = [h_1(x), h_2(x), \dots, h_j(x), \dots, h_m(x)]^T \in \mathbb{R}^m$, m is the number of RBFNN's hidden layer nodes. Using Gaussian basis functions, $h_j(x)$ can be expressed as follows

$$h_j(x) = \exp \left(-\frac{x - c_j^2}{2b_j^2} \right), j = 1, 2, \dots, m \quad (17)$$

where c_j is the j th center parameter of RBFNN, $c_j = [c_{j1}, c_{j2}, \dots, c_{jq}]^T$. $b_j > 0$ is the j th wide parameter of RBFNN. $W^* = [W_1^*, W_2^*, W_3^*, W_4^*, W_5^*, W_6^*] \in \mathbb{R}^{m \times 6}$ is the desired hidden-to-output layer interconnection weighted matrix. $\mu \in \mathbb{R}^6$ is the RBFNN estimation error and $\|\mu\| \leq \mu^*$, μ^* is an unknown positive constant. The desired weighted matrix $W \in \mathbb{R}^{m \times 6}$ can be defined as

$$W^* = \arg \min_{W \in \mathbb{R}^{m \times 6}} \left\{ \sup_{x \in \mathcal{Q}_x} \|D - W^T h(x)\| \right\} \quad (18)$$

The input vector of RBFNN can be defined as $x = [e^T, \dot{e}^T]^T$, then estimation value of the uncertain nonlinearity D can be written as follows

$$\hat{D} = \hat{W}^T h(x) \quad (19)$$

where $\hat{W} = [\hat{W}_1, \hat{W}_2, \hat{W}_3, \hat{W}_4, \hat{W}_5, \hat{W}_6]$ is the estimation value of the weighted matrix W^* .

To consider unknown upper bounds μ^* of approximation error, we propose the adaptive control law as follows

$$u = H^{-1} \left(-A - R^{-1}L - \hat{D} - \hat{\mu}^2 \frac{\|s\|}{\hat{\mu}\|s\| + \sigma} - K_2s \right) \quad (20)$$

$$\dot{\hat{W}}_i = \tau_{wi}[s_i h(x) - \beta \hat{W}_i], \quad i = 1, 2, 3, 4, 5, 6 \quad (21)$$

$$\dot{\hat{\mu}} = \tau_\mu(\|s\| - \gamma \hat{\mu}) \quad (22)$$

where $\hat{\mu}$ denotes the estimation value of the upper bounds μ^* , $K_2 > 0$, $\sigma > 0$, $\tau_{wi} > 0$, $\beta > 0$, $\tau_\mu > 0$, and $\gamma > 0$ are designed control parameters and adaptive gains, respectively.

Theorem 1. For the error system (15) from OBFN dynamic model (3) by the error transformation equation (9), according to the control law (20) and adaptive laws (21) and (22), the transforming error ε_i and tracking error e_i can be guaranteed uniformly ultimately bounded and satisfy prescribed performance equation (6), respectively.

Proof. Based on symmetric positive definite and bounded characteristics of matrix R , we consider the Lyapunov function candidate.

$$V = \frac{1}{2}s^T R^{-1}s + \frac{1}{2}\text{tr}(\tilde{W}^T \Gamma_w^{-1} \tilde{W}) + \frac{1}{2} \cdot \frac{1}{\tau_\mu} \tilde{\mu}^2 \quad (23)$$

where $\tilde{W} = \hat{W} - W^*$, $\tilde{\mu} = \hat{\mu} - \mu^*$ are estimation errors, $\Gamma_w = \text{diag}[\tau_{w1}, \tau_{w2}, \tau_{w3}, \tau_{w4}, \tau_{w5}, \tau_{w6}]$. Differentiating V with respect to time and substituting equations (15) and (20) to (22) into it, we obtain

$$\begin{aligned} \dot{V} &= s^T R^{-1} \dot{s} + \text{tr}(\tilde{W}^T \Gamma_w^{-1} \dot{\tilde{W}}) + \frac{1}{\tau_\mu} \tilde{\mu} \dot{\tilde{\mu}} \\ &= s^T R^{-1} [Q + R(A + Hu + D)] + \sum_{i=1}^6 \frac{1}{\tau_{wi}} \tilde{W}_i^T \dot{\tilde{W}}_i + \frac{1}{\tau_\mu} \tilde{\mu} \dot{\tilde{\mu}} \\ &= s^T \left[-\tilde{W}^T h(x) + \mu - \frac{\hat{\mu}^2 s}{\hat{\mu} s + \sigma} - K_2 s \right] \\ &\quad + \sum_{i=1}^6 \tilde{W}_i^T [s_i h(x) - \beta \hat{W}_i] + \tilde{\mu} (s - \gamma \hat{\mu}) \\ &\leq -s^T K_2 s + s \hat{\mu} - \frac{\hat{\mu}^2 s^2}{\hat{\mu} s + \sigma} - \beta \sum_{i=1}^6 \tilde{W}_i^T \hat{W}_i - \gamma \tilde{\mu} \hat{\mu} \end{aligned} \quad (24)$$

Applying Young's inequality, we obtain

$$-\beta \sum_{i=1}^6 \tilde{W}_i^T \hat{W}_i \leq \frac{1}{2} \beta \sum_{i=1}^6 \tilde{W}_i^T \tilde{W}_i + \frac{1}{2} \beta \sum_{i=1}^6 W_i^{*T} W_i^* \quad (25)$$

$$-\gamma \tilde{\mu} \hat{\mu} \leq -\frac{1}{2} \gamma \tilde{\mu}^2 + \frac{1}{2} \gamma \mu^{*2} \quad (26)$$

By adaptive law (22), we can have $\hat{\mu} > 0$, then

$$\|s\| \hat{\mu} - \frac{\hat{\mu}^2 \|s\|^2}{\hat{\mu} \|s\| + \sigma} = (\hat{\mu} \|s\|) \cdot \frac{\sigma}{\hat{\mu} \|s\| + \sigma} < \sigma \quad (27)$$

To further simplify equation (24), one has that

$$\begin{aligned} \dot{V} &\leq -s^T K_2 s - \frac{1}{2} \beta \sum_{i=1}^6 \tilde{W}_i^T \tilde{W}_i - \frac{1}{2} \gamma \tilde{\mu}^2 + \frac{1}{2} \beta \sum_{i=1}^6 W_i^{*T} W_i^* \\ &\quad + \frac{1}{2} \gamma \mu^{*2} + \sigma \end{aligned} \quad (28)$$

Let $\kappa = \frac{1}{2} \beta \sum_{i=1}^6 W_i^{*T} W_i^* + \frac{1}{2} \gamma \mu^{*2} + \sigma$. $\dot{V} \leq 0$ when $\|s\| > \sqrt{\kappa / \lambda_{\min}(K_2)}$ or $\|\tilde{W}_i\| > \sqrt{2\kappa / \beta}$ or $|\tilde{\mu}| > \sqrt{2\kappa / \gamma}$. Thus, the variable s , the matrix \tilde{W}_i , and estimation error $\tilde{\mu}$ are uniformly ultimately bounded with respect to the sets

$$\begin{aligned} N_1 &= \{s \in \mathbb{R}^6 : s \leq \sqrt{\kappa / \lambda_{\min}(K_2)}\} \\ N_2 &= \{\tilde{W}_i \in \mathbb{R}^m : \tilde{W}_i \leq \sqrt{2\kappa / \beta}\} \\ N_3 &= \{\tilde{\mu} \in \mathbb{R} : \tilde{\mu} \leq \sqrt{2\kappa / \gamma}\} \end{aligned} \quad (29)$$

where, $\lambda_{\min}(K_2)$ denotes minimal eigenvalue of the matrix K_2 . The transforming error is uniformly ultimately bounded with respect to the set

$$N_4 = \{\varepsilon_i \in \mathbb{R} : \varepsilon_i \leq \sqrt{\kappa / \lambda_{\min}(K_2)} / \lambda_i\} \quad (30)$$

Owing to the smooth and strictly increasing property of the $S_i(\varepsilon_i)$, the performance constraint equation (6) is obtained. It means the tracking error e_i achieves prescribed dynamic performance and steady-state response.

Remark 4. According to the definition of prescribed performance method and the proof of theorem 1, we give the guidelines on how to choose appropriate parameters and gains of performance function (5), RBFNN (equation (17)), and control strategy (equations (20) to (22)) in practical applications as follows.

- (1) The parameters ρ_{i0} , $\rho_{i\infty}$, and k_i of performance function should be selected to satisfy practical mission requirements. Especially, ρ_{i0} needs meet the initial conditions of the trajectory tracking control system.
- (2) The number of the RBFNN hidden nodes is approximately seven and the matrix of the RBFNN center needs to be symmetric.
- (3) The parameter σ and matrix λ of controller and adaptive gains β and γ should be small enough. Additionally, the choice of the matrix K_2 and adaptive gains τ_{wi} and τ_μ is not specified.

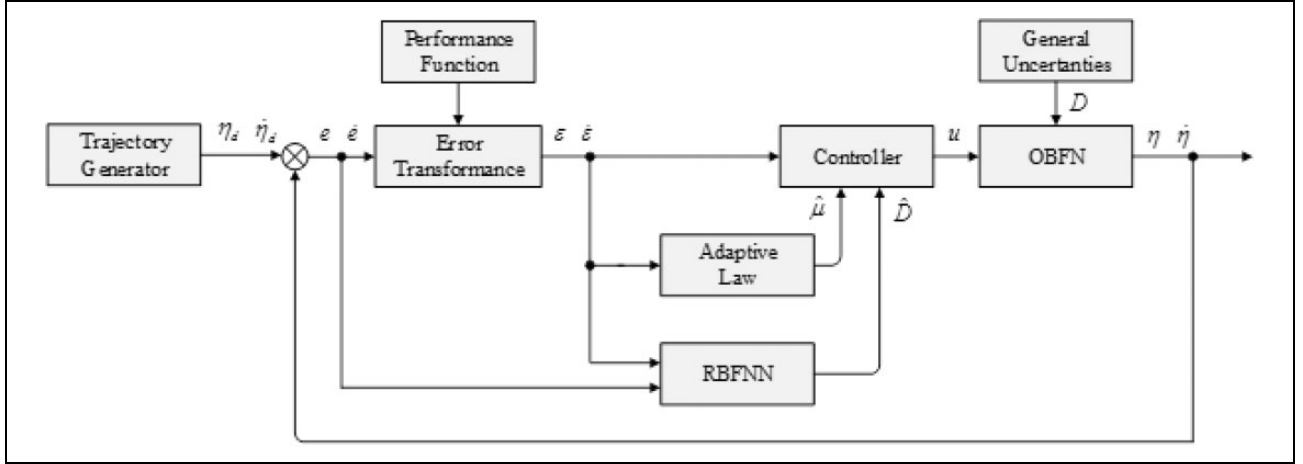


Figure 2. Schematic of the proposed trajectory tracking control system. OBFN: ocean bottom flying node; RBFNN: radial basis function neural network.

The structure of the trajectory tracking control system with proposed prescribed performance approaches is illustrated in Figure 2.

Numerical simulations and comparisons

To verify the effectiveness of the proposed control method, the simulations are applied to the OBFN system which considers ocean current disturbances and model uncertainties as well as thruster faults. The hydrodynamic parameters, inertia coefficients, and the initial values of η are shown in Tables 1 to 3, respectively.

Model uncertainty

The model uncertainties are quantified for convenience in this article. Twenty percent nominal values serve as model error and consider it as a part of the disturbance in the simulation.

Ocean current disturbance

A first-order Gauss–Markov process is applied in simulation to represent ocean current disturbance, denoted as follows³⁵

$$\dot{V}_c + \mu V_c = \omega \quad (31)$$

where V_c is the speed of ocean current in the earth coordinate system, ω is Gaussian white noise where mean is 1, variance is 1, and $\mu = 3$. In this study, we assume that the direction of ocean current parallels the x -axis positive direction in the earth coordinate system.

Thruster fault

Thruster configuration of the OBFN is adopted in the fully-actuated form, as shown in Figure 3.

Table 1. The hydrodynamic parameters of the OBFN.

Name	Coefficients	Value
Surge	$X\dot{u}/\text{kg}$	40.6
	$X_u/\text{kg} \cdot \text{s}^{-1}$	21.9
	$X_{u u }/\text{kg} \cdot \text{m}^{-1}$	24.5
Lateral	$Y\dot{v}/\text{kg}$	82.3
	$Y_v/\text{kg} \cdot \text{s}^{-1}$	47.4
	$Y_{v v }/\text{kg} \cdot \text{m}^{-1}$	34.7
Heave	$Z\dot{w}/\text{kg}$	114.6
	$Z_w/\text{kg} \cdot \text{s}^{-1}$	53.5
	$Z_{w w }/\text{kg} \cdot \text{m}^{-1}$	40.2
Yaw	$N\dot{r}/\text{kg} \cdot \text{m}^2$	59.1
	$N_r/\text{kg} \cdot \text{m}^2 \cdot \text{s}^{-1}$	86.9
	$N_{r r }/\text{kg} \cdot \text{m}^2$	39.3
Roll	$K\dot{p}/\text{kg} \cdot \text{m}^2$	55.7
	$K_p/\text{kg} \cdot \text{m}^2 \cdot \text{s}^{-1}$	71.9
	$K_{p p }/\text{kg} \cdot \text{m}^2$	42.1
Pitch	$M\dot{q}/\text{kg} \cdot \text{m}^2$	76.5
	$M_q/\text{kg} \cdot \text{m}^2 \cdot \text{s}^{-1}$	97.3
	$M_{q q }/\text{kg} \cdot \text{m}^2$	48.3

OBFN: ocean bottom flying node.

From Figure 3, it can be found that the thruster configurations are the same in each direction. Therefore, we consider that the fault only occurred in the thruster T-1, which can represent any thruster fault form. Two kinds of thruster faults for the thruster T-1 can be expressed as²⁴

$$k_{11} = \begin{cases} 0 & t < 30 \\ -0.5 & t \geq 30 \end{cases} \quad (32)$$

$$k_{12} = \begin{cases} 0 & t < 15 \\ -0.5(1 - \exp(-(t - 15)/5)) & t \geq 15 \end{cases} \quad (33)$$

where equations (32) and (33) represent abrupt and incipient thruster fault cases, respectively.

Table 2. The inertia coefficients of the OBFN.

Mass (kg)	$I_x(\text{Nms}^2)$	$I_y(\text{Nms}^2)$	$I_z(\text{Nms}^2)$	$I_{xy}(\text{Nms}^2)$	$I_{yz}(\text{Nms}^2)$	$I_{xz}(\text{Nms}^2)$
92	49	84	79	0	0	0

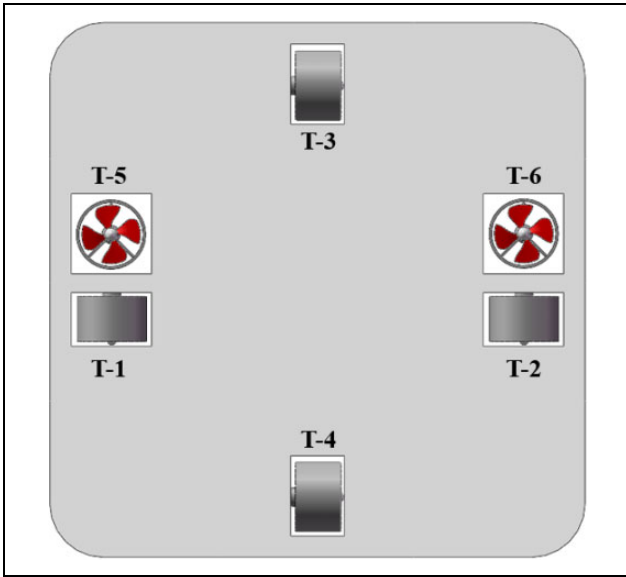
OBFN: ocean bottom flying node.

Table 3. The initial values of η .

x(m)	y(m)	z(m)	ϕ (rad)	θ (rad)	ψ (rad)
0.02	0	0.01	0	0	0

Table 4. Parameters of the prescribed performance function.

Parameters	ρ_{i0}	$\rho_{i\infty}$	k_i	δ_i
Values	1.6	0.0035	0.15	0.2

**Figure 3.** Thruster configuration of the OBFN. OBFN: ocean bottom flying node

Parameters of the controller

The simulation requires that the OBFN trajectory tracking precision should be limited into the range of 0.0035. Therefore, desired trajectory tracking control performance for the OBFN can be designed as follows:

- (1) Steady-state tracking error is limited into the range of 0.0035;
- (2) convergent speed is faster than $e^{-0.15t}$;
- (3) system response has no overshoot.

The performance function $\rho_i(t)$ and parameter δ_i are given in Table 4.

The controller parameters can be denoted as $\lambda = \text{diag}[0.125, 0.125, 0.125, 0.125, 0.125, 0.125]$, $K_2 = \text{diag}[0.6, 0.6, 0.6, 0.6, 0.6, 0.6]$, $\sigma = 0.01$. Adaptive gains can be chosen as $\tau_{wi} = \tau_{\mu} = 0.5$, $\beta = \gamma = 0.01$. The number of the RBFNN hidden nodes can be designed as $j = 7$, $b_j = 0.09$. The center parameter of RBFNN is $c = [c_1, \dots, c_7]$, which can be expressed as follows

$$c = \begin{bmatrix} -0.3 & -0.17 & -0.08 & 0 & 0.08 & 0.17 & 0.3 \\ -0.15 & -0.1 & -0.05 & 0 & 0.05 & 0.1 & 0.15 \\ -0.2 & -0.13 & -0.07 & 0 & 0.07 & 0.13 & 0.2 \\ -0.03 & -0.02 & -0.01 & 0 & 0.01 & 0.02 & 0.03 \\ -0.15 & -0.1 & -0.05 & 0 & 0.05 & 0.1 & 0.15 \\ -0.03 & -0.02 & -0.01 & 0 & 0.01 & 0.02 & 0.03 \\ -0.3 & -0.17 & -0.08 & 0 & 0.08 & 0.17 & 0.3 \\ -0.15 & -0.1 & -0.05 & 0 & 0.05 & 0.1 & 0.15 \\ -0.2 & -0.13 & -0.07 & 0 & 0.07 & 0.13 & 0.2 \\ -0.03 & -0.02 & -0.01 & 0 & 0.01 & 0.02 & 0.03 \\ -0.15 & -0.1 & -0.05 & 0 & 0.05 & 0.1 & 0.15 \\ -0.03 & -0.02 & -0.01 & 0 & 0.01 & 0.02 & 0.03 \end{bmatrix} \quad (34)$$

After the supporting ship arrives at the target exploration area, OBFNs are successively detached from the geophysical vessel. Then the OBFN needs to overcome the influence of ocean current and track predefined trajectory to arrive at target points. The downward spiral is beneficial to dive the AUV deep in a small area. Therefore, this study chooses a spiral trajectory as the desired trajectory, expressed as follows

$$x_d = 2\sin(0.1t), y_d = 2\cos(0.1t) + 2, z_d = -0.5144t$$

$$\phi_d = 0, \theta_d = 0, \psi_d = 0$$

$$\eta_d = [x_d; y_d; z_d; \phi_d; \theta_d; \psi_d]$$

We simulate for two different thruster fault cases of the OBFN. Besides, to make comparative study, we compare the proposed control algorithm (equations (20) to (22)) with a non-prescribed-performance controller with the same control structure and parameters. This controller can be called adaptive tracking controller (ATC) and is expressed as equations (35) to (37).

$$u = H^{-1} \left(-A + \ddot{\eta}_d - \lambda \dot{e} - \hat{D} - \hat{\mu}^2 \frac{s_e}{\hat{\mu} \|s_e\| + \sigma} - K_2 s \right) \quad (35)$$

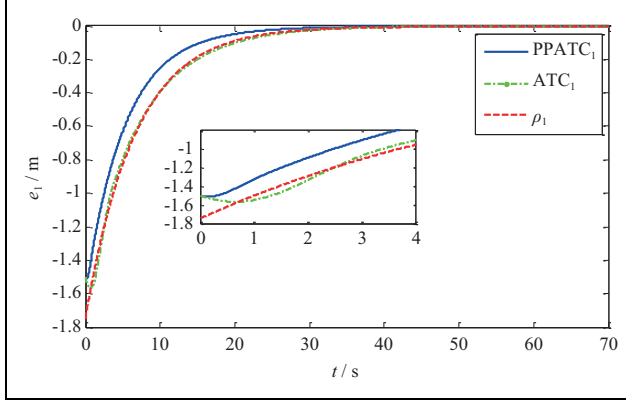


Figure 4. Tracking error in surge e_1 with thruster abrupt fault. PPATC: prescribed performance adaptive tracking controller; ATC: adaptive tracking controller.

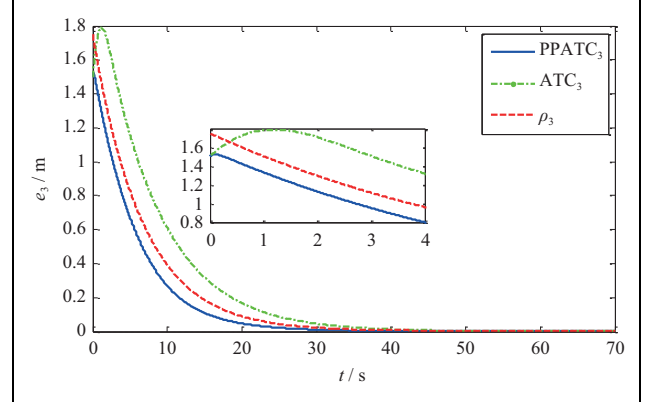


Figure 6. Tracking error in heave e_3 with thruster abrupt fault. PPATC: prescribed performance adaptive tracking controller; ATC: adaptive tracking controller.

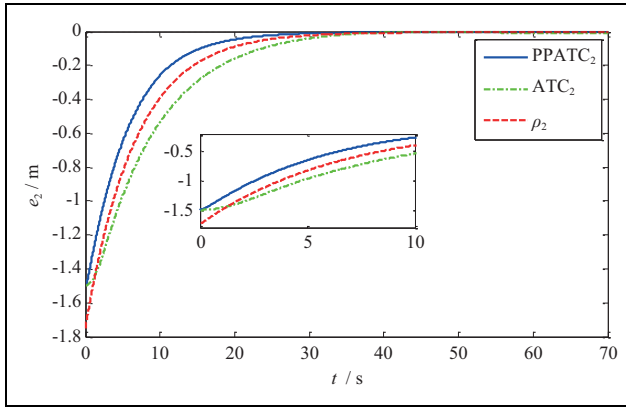


Figure 5. Tracking error in lateral e_2 with thruster abrupt fault. PPATC: prescribed performance adaptive tracking controller; ATC: adaptive tracking controller.

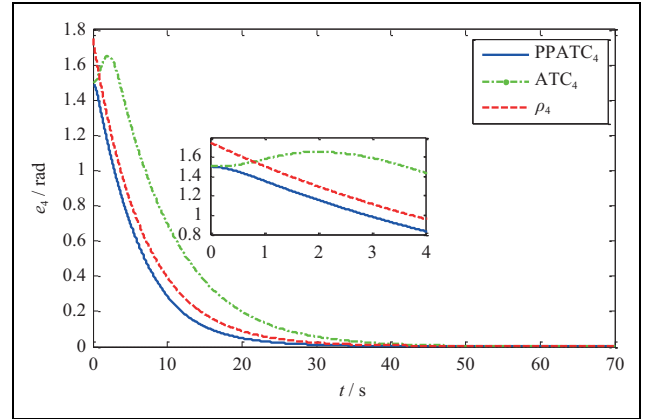


Figure 7. Tracking error in roll e_4 with thruster abrupt fault. PPATC: prescribed performance adaptive tracking controller; ATC: adaptive tracking controller.

$$\dot{\hat{W}}_i = \tau_{wi} [s_{ei} h(x) - \beta \hat{W}_i], i = 1, 2, 3, 4, 5, 6 \quad (36)$$

$$\dot{\hat{\mu}} = \tau_{\mu} (||s_e|| - \gamma \hat{\mu}) \quad (37)$$

where $s_e = [s_{e1}, s_{e2}, s_{e3}, s_{e4}, s_{e5}, s_{e6}]^T = \lambda e + \dot{e}$.

Case 1: Abrupt thruster fault case

In this part, thruster fault is based on equation (21). Figures 4–9 represent 6-DOF trajectory tracking error of the OBFN. The prescribed performance adaptive tracking controller (equations (20) to (22)) is denoted as PPATC, the adaptive tracking controller (equations (35) to (37)) is denoted as ATC, and the prescribed performance bounds are denoted as ρ . The comparisons on actual and desired 3-D trajectories figure is shown in Figure 10. The control input of the OBFN is shown in Figure 11.

From Figures 4 to 9, it can be found that the proposed PPATC control method (equations (20) to (22)) could keep the trajectory tracking error in prescribed performance bounds and obtain desired transient and steady responses.

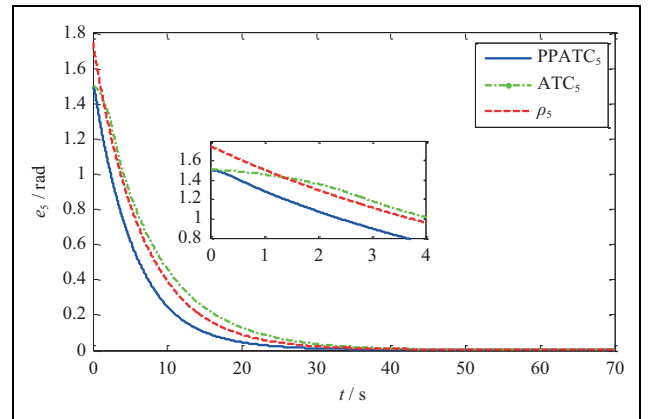


Figure 8. Tracking error in pitch e_5 with thruster abrupt fault. PPATC: prescribed performance adaptive tracking controller; ATC: adaptive tracking controller.

However, the ATC control strategy with the same parameters cannot meet predefined precision and has obvious overshoot. The simulation results indicate that the

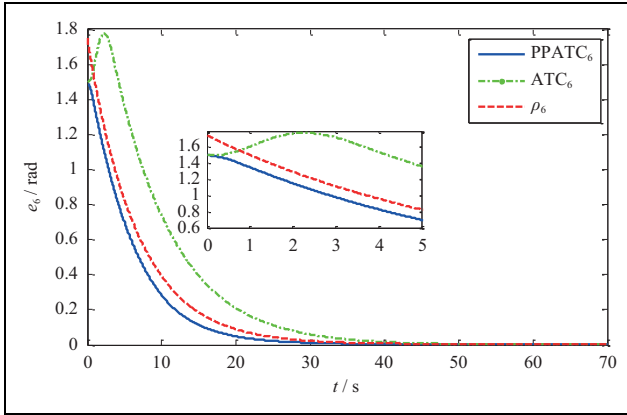


Figure 9. Tracking error in yaw e_6 with thruster abrupt fault. PPATC: prescribed performance adaptive tracking controller; ATC: adaptive tracking controller.

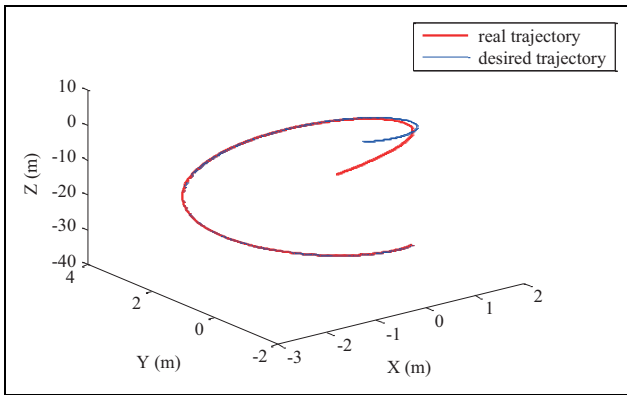


Figure 10. The real and desired trajectories in the simulation case 1.

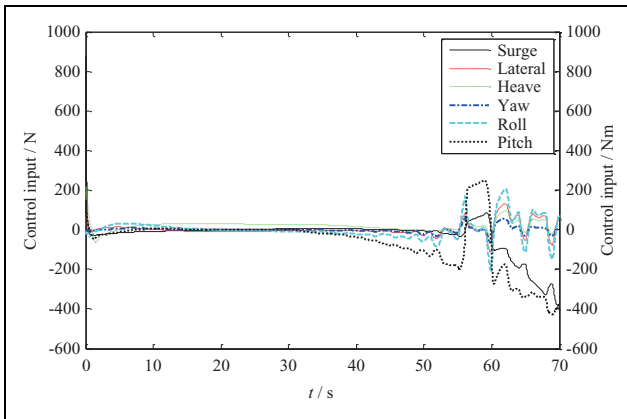


Figure 11. The control input of the OBFN. OBFN: ocean bottom flying node.

prescribed performance method could make the tracking error achieve desired control requirements.

Remark 5. The simulation experiment results based on different thruster saturation values show that system trajectory

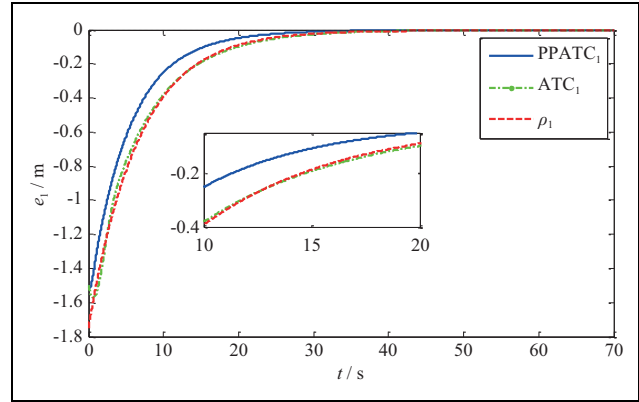


Figure 12. Tracking error in surge e_1 with thruster incipient fault. PPATC: prescribed performance adaptive tracking controller; ATC: adaptive tracking controller.

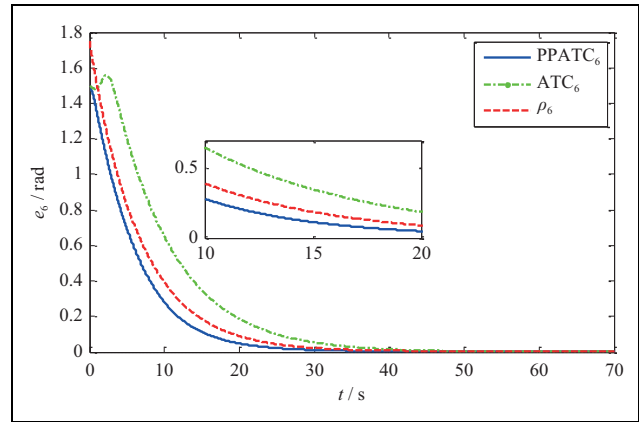


Figure 13. Tracking error in yaw e_6 with thruster incipient fault. PPATC: prescribed performance adaptive tracking controller; ATC: adaptive tracking controller.

tracking error is not restricted to prescribed bounds when the control input is below 370 N/Nm. Therefore, the proposed control method achieves prescribed dynamic performance and steady state response under the moderate thruster saturation. How to extend the control method of this article to more general thruster saturation application may be an interesting issue. This issue will be solved in the future work.

Case 2: Incipient thruster fault case

Similar to the abrupt thruster fault case, we choose the thruster fault based on equation (33) in this part. Since the simulation results are similar to those in case 1, this section only provides surge and yaw trajectory tracking errors which are direct correlation to thruster T-1 fault. The simulation results are shown in Figures 12 and 13, and the definitions of curves is the same as those in case 1. The corresponding comparisons on actual and desired 3-D trajectories figure is shown in Figure 14.

From Figures 12 and 13, we can obtain similar conclusions that the proposed PPATC control method is still

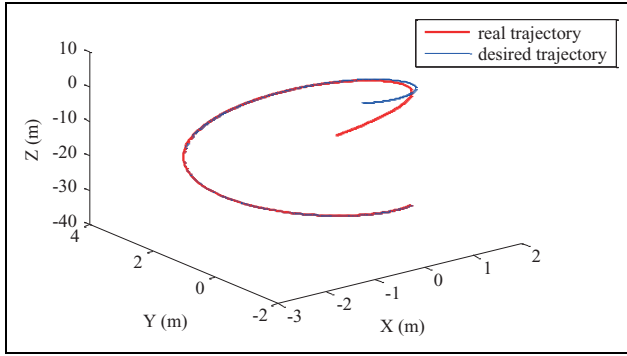


Figure 14. The real and desired trajectories in the simulation case 2.

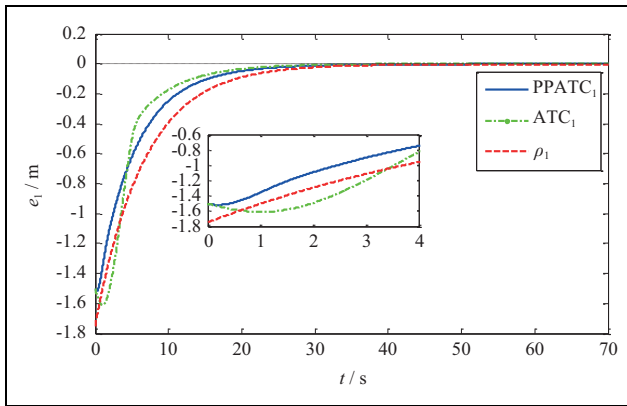


Figure 15. Tracking error in surge e_1 with low gain. PPATC: prescribed performance adaptive tracking controller; ATC: adaptive tracking controller.

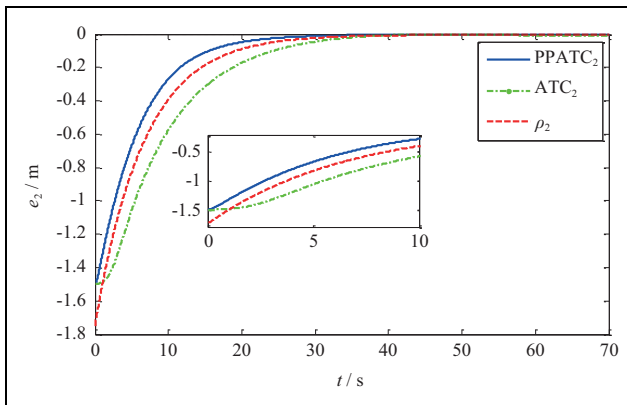


Figure 16. Tracking error in lateral e_2 with low gain. PPATC: prescribed performance adaptive tracking controller; ATC: adaptive tracking controller.

effective in thruster incipient fault case and has better control performances than the ATC algorithm with the same control parameters.

To verify that the proposed PPATC control method has less dependence on the control parameters, extra simulations are performed with the control gains chosen as the

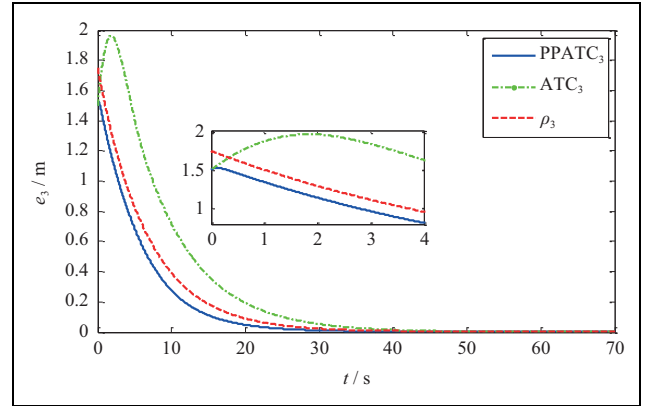


Figure 17. Tracking error in heave e_3 with low gain. PPATC: prescribed performance adaptive tracking controller; ATC: adaptive tracking controller.

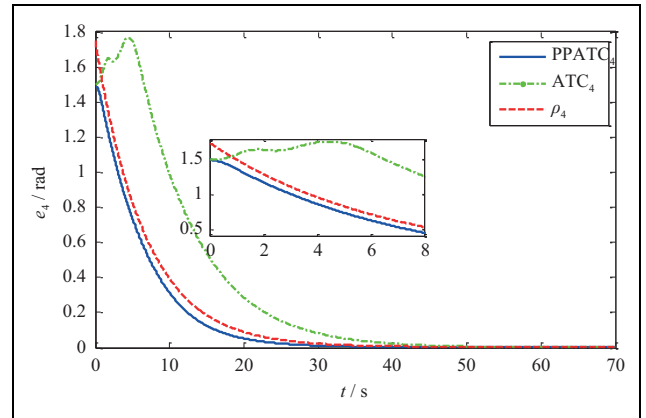


Figure 18. Tracking error in roll e_4 with low gain. PPATC: prescribed performance adaptive tracking controller; ATC: adaptive tracking controller.

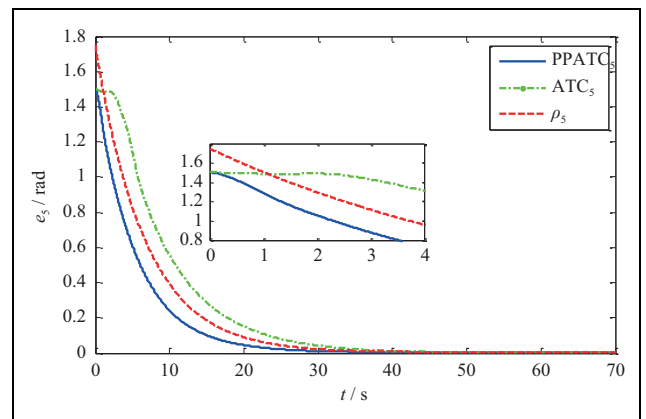


Figure 19. Tracking error in pitch e_5 with low gain. PPATC: prescribed performance adaptive tracking controller; ATC: adaptive tracking controller.

half values of the original ones. The abrupt thruster fault case is considered. The simulation results are shown in Figures 15 to 20. Comparing with Figures 4 to 9, we can

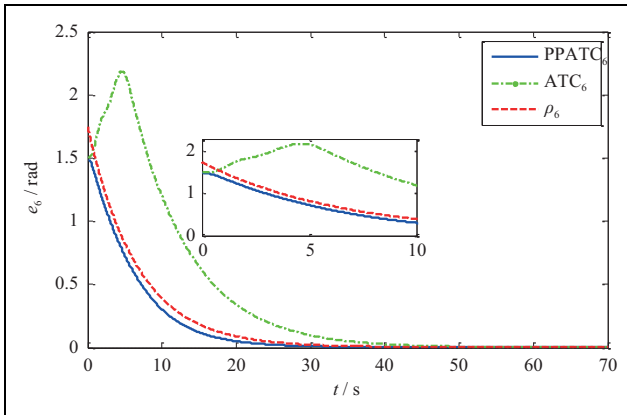


Figure 20. Tracking error in yaw e_6 with low gain. PPATC: prescribed performance adaptive tracking controller; ATC: adaptive tracking controller.

obtain that the control performance of the PPATC control method has no obvious change while the tracking performance of the ATC control strategy becomes worse than that before the control gains reduction. Therefore, the proposed PPATC control method has less dependence on the control gains and better system robustness.

Conclusion

In this article, trajectory tracking control of the OBFN with ocean current disturbances, model uncertainties, and thruster faults has been addressed by combining prescribed performance technique with RBFNN approximation system. To take into account the influence caused by disturbances, uncertainties, and faults, the system general uncertainties has been introduced to summarize them. The RBFNN approximation system was adopted to approximate the general uncertainties, and the upper bound of the approximate error was estimated by adaptive method. Based on the performance function and an error transformation, the OBFN trajectory tracking error was restricted to prescribed bounds to ensure expect performance that the convergence rate, overshoot, and steady precision can be predefined. The simulation results for two types of thruster faults indicated that the proposed control method can effectively restrain the effect of the general uncertainties while obtaining an expected trajectory tracking performance with less dependence on the control parameters.


Declaration of conflicting interests


The author(s) declared no potential conflicts of interest with respect to the research, authorship, and/or publication of this article.

Funding

The author(s) disclosed receipt of following financial support for the research, authorship, and/or publication of this article: This work was supported by the National Natural Science Foundation of China, under grant (Nos.U1713205 and 61803119).

ORCID iD

Hongde Qin  <https://orcid.org/0000-0002-9794-4491>

Yanchao Sun  <https://orcid.org/0000-0001-7392-4472>

Reference

1. Bidoki M, Mortazavi M, and Sabzehparvar M. A new approach in system and tactic design optimization of an autonomous underwater vehicle by using multidisciplinary design optimization. *Ocean Eng* 2018; 147: 517–530.
2. Wang N, Xie G, Pan X, et al. Full-state regulation control of asymmetric underactuated surface vehicles. *IEEE Trans Ind Electron* 2018; pp. 1–1. DOI: 10.1109/TIE.2018.2890500.
3. Wynn RB, Huvenne VAI, Bas TPL, et al. Autonomous underwater vehicles (AUVs): their past, present and future contributions to the advancement of marine geoscience. *Mar Geol* 2014; 352(2): 451–468.
4. Shukla A and Karki H. Application of robotics in offshore oil and gas industry—a review part II. *Rob Auton Syst* 2015; 75(PB): 508–524.
5. Carreras M, Hernández JD, Vidal E, et al. Sparus II AUV—a hovering vehicle for seabed inspection. *IEEE J Ocean Eng* 2018; 43(2): 344–355.
6. Allotta B, Costanzi R, Pugi L, et al. Identification of the main hydrodynamic parameters of Typhoon AUV from a reduced experimental dataset. *Ocean Eng* 2018; 147: 77–88.
7. Elmokadem T, Zribi M, and Youcef-Toumi K. Trajectory tracking sliding mode control of underactuated AUVs. *Non-linear Dyn* 2016; 84(2): 1079–1091.
8. Shen C, Shi Y, and Buckham B. Trajectory tracking control of an autonomous underwater vehicle using Lyapunov-based model predictive control. *IEEE Trans Ind Electron* 2018; 65(7): 5796–5805.
9. Bi FY, Wei YJ, Zhang JZ, et al. Position-tracking control of underactuated autonomous underwater vehicles in the presence of unknown ocean currents. *IET Control Theory Appl* 2010; 4(11): 2369–2380.
10. Kokegei M, He F, and Sammut K. Fully coupled 6 degrees-of-freedom control of autonomous underwater vehicles: *Oceans 2008*. Quebec City: IEEE, Quebec City, QC, Canada, 15–18 September 2008, pp. 1–7.
11. Qiao L and Zhang W. Double-loop integral terminal sliding mode tracking control for UUVs with adaptive dynamic compensation of uncertainties and disturbances. *IEEE J Ocean Eng* 2018; 44(1): 29–53.
12. Qiao L and Zhang W. Adaptive second-order fast nonsingular terminal sliding mode tracking control for fully actuated autonomous underwater vehicles. *IEEE J Oceanic Eng* 2018: 1–23.
13. Londhe PS, Dhadekar DD, Patre BM, et al. Non-singular terminal sliding mode control for robust trajectory tracking control of an autonomous underwater vehicle. In: *Indian control conference*, Guwahati, India, 4–6 January 2017, pp. 443–449.
14. Wang N, Sun JC, and Meng JE. Tracking-error-based universal adaptive fuzzy control for output tracking of nonlinear

- systems with completely unknown dynamics. *IEEE Trans Fuzzy Syst* 2018; 26(2): 869–883.
15. Rout R and Subudhi B. Inverse optimal self-tuning PID control design for an autonomous underwater vehicle. *Int J Syst Sci* 2016; 48(2): 367–375.
 16. Wang N, Su SF, Yin J, et al. Global asymptotic model-free trajectory-independent tracking control of an uncertain marine vehicle: an adaptive universe-based fuzzy control approach. *IEEE Trans Fuzzy Syst* 2018; 26(3): 1613–1625.
 17. Karkoub M, Wu HM, and Hwang CL. Nonlinear trajectory-tracking control of an autonomous underwater vehicle. *Ocean Eng* 2017; 145: 188–198.
 18. Wang N, Sun JC, Han M, et al. Adaptive approximation-based regulation control for a class of uncertain nonlinear systems without feedback linearizability. *IEEE Trans Neural Networks Learn Syst* 2017; 29(8): 3747–3760.
 19. Lakhekar GV and Waghmare LM. Robust maneuvering of autonomous underwater vehicle: an adaptive fuzzy PI sliding mode control. *Intel Serv Robot* 2017; 10(3): 1–18.
 20. Wang N, Sun Z, Yin JC, et al. Fuzzy unknown observer-based robust adaptive path following control of underactuated surface vehicles subject to multiple unknowns. *Ocean Eng* 2019; 176: 57–64.
 21. Sun B, Zhu D, and Yang SX. A novel tracking controller for autonomous underwater vehicles with thruster fault accommodation. *J Navig* 2016; 69(3): 593–612.
 22. Ahmadzadeh SR, Kormushev P, and Caldwell DG. Multi-objective reinforcement learning for AUV thruster failure recovery. In: *2014 IEEE symposium on adaptive dynamic programming and reinforcement learning*, Orlando, FL, USA, 9–12 December 2014, pp. 1–8. Orlando: IEEE.
 23. Davoodi MR, Meskin N, and Khorasani K. Simultaneous fault detection, isolation and control tracking design using a single observer-based module. In: *American control conference*, Portland, USA, June 2014, pp. 3047–3052. New York, NY, USA: IEEE.
 24. Wang Y, Zhang M, Wilson PA, et al. Adaptive neural network-based backstepping fault tolerant control for underwater vehicles with thruster fault. *Ocean Eng* 2015; 110: 15–24.
 25. Zhang M, Liu X, Yin B, et al. Adaptive terminal sliding mode based thruster fault tolerant control for underwater vehicle in time-varying ocean currents. *J Franklin Inst* 2015; 352(11): 4935–4961.
 26. Zhang M, Liu X, and Wang F. Backstepping based adaptive region tracking fault tolerant control for autonomous underwater vehicles. *J Navig* 2016; 70(1): 184–204.
 27. Bechlioulis CP and Rovithakis GA. Robust adaptive control of feedback linearizable MIMO nonlinear systems with prescribed performance. *IEEE Trans Autom Control* 2008; 53(9): 2090–2099.
 28. Na J, Chen Q, Ren X, et al. Adaptive prescribed performance motion control of servo mechanisms with friction compensation. *IEEE Trans Ind Electron* 2013; 61(1): 486–494.
 29. Bu X, Wu X, Zhu F, et al. Novel prescribed performance neural control of a flexible air-breathing hypersonic vehicle with unknown initial errors. *ISA Trans* 2015; 59: 149–59.
 30. Sui S, Tong S, and Li Y. Observer-based fuzzy adaptive prescribed performance tracking control for nonlinear stochastic systems with input saturation. *Neurocomputing* 2015; 158: 100–108.
 31. Bechlioulis CP, Karras GC, Heshmati-Alamdari S, et al. Trajectory tracking with prescribed performance for underactuated underwater vehicles under model uncertainties and external disturbances. *IEEE Trans Control Syst Technol* 2017; 25(2): 429–440.
 32. Mohapatra AK, Gautam N, and Gibson RL. Combined routing and node replacement in energy-efficient underwater sensor networks for seismic monitoring. *IEEE J Ocean Eng* 2013; 38(1): 80–90.
 33. Sil S, Srivastava RP, and Sen MK. Observation of shear-wave splitting in the multicomponent node data from Atlantis field, Gulf of Mexico. *Geophys Prospect* 2010; 58(6): 953–964.
 34. Operto S, Miniussi A, Brossier R, et al. Efficient 3-D frequency-domain mono-parameter full-waveform inversion of ocean-bottom cable data: application to Valhall in the visco-acoustic vertical transverse isotropic approximation. *Geophys J Int* 2015; 202(2): 1362–1391.
 35. Fossen TI. *Handbook of marine craft hydrodynamics and motion control*, 1st ed. New York: John Wiley and Sons, 2011.
 36. Omerdic E and Roberts G. Thruster fault diagnosis and accommodation for open-frame underwater vehicles. *Control Eng Pract* 2004; 12(12): 1575–1598.
 37. Zhang C, Sun YC, Ma GF, et al. Prescribed performance adaptive attitude tracking control for flexible spacecraft. *J Harbin Inst Technol* 2018; 50(4): 1–7.